Chapter III: Fabrication of Fiber Bragg Grating

3.1 Introduction

Fiber Bragg gratings can be produced in photosensitive optical fibers by exposure to pulsed [1] or continuous wave (CW) [2] ultra violet (UV) light in the wavelength band of 240 to 260nm. The commonly used techniques for fabricating such short period fiber Bragg gratings (FBGs) are interferometric, point by point writing and phase mask printing [3][4][5]. For interferometric technique, the UV beam is divided into two at a beam splitter and brought together at a mutual angle, by reflections from two mirrors. The interferometric technique is quite complicated and alignment sensitive especially when gratings have to be written precisely for a specific wavelength. In the point by point writing technique, each writing plane is written into a fiber separately by a focused single laser pulse, consequently this technique requires a precise translation stage. The phase mask printing technique is a simpler approach where a mask with a phase grating can be used to generate two laser beams.

In this chapter, a technique to fabricate a high reflectivity FBG with minimal optics is described. The FBG is written on high-germania boron co-doped optical fiber using a uniform phase mask with a 244nm continuous wave UV light.

3.2 Experimental set up

A schematic of the FBG writing set up is shown in Figure 3.1. The output of a CW argon ion laser operating at λ = 244nm is reflected by a mirror, expanded with the two circular lenses, focused with cylindrical lens, and then passed through a phase

mask before the fiber is irradiated. The circular lenses have a focal length of approximately 5cm and 50cm, and are separated to each other by 45cm thus making a beam expander telescope. The phase mask is used to generate two interfering beams close to the fiber as shown in Figure 3.2. The phase mask, specially made for a particular UV wavelength is placed just alongside a bare fiber with its mask patterns perpendicular to the fiber. The fiber jacket is stripped about 5 cm along the place where inscription is to occur. After being set perpendicularly to the phase mask edge, the fiber is clamped on two supports, placed on either side of the fringe pattern, separated by 6 cm. The supports are mounted on a precision translation stage that allowed its separation from the phase mask to be adjusted. The fiber should be placed in near contact with the fine corrugations of the phase mask before writing. The separation of the fiber core from phase mask is checked via naked eye and it should be less than 0.1mm. This separation is a critical parameter in producing quality FBGs. However, placing the fiber in contact with the fine corrugations is not desirable due to possible damage to the phase mask. Details of the alignment procedure are presented in next section.

The FBGs are inscribed in single mode high-germania boron co-doped fibers. The generated spectral transmission of the FBG was recorded in real time in the course of photoimprinting, using a broadband source from a fiber amplifier and an optical spectrum analyzer. The real time need for monitoring is essential in order to avoid the grating being formed with a saturated exposure, which affects the spectrum and reflectivity. It also allows for the determination of the fiber property. Shown in Pic.3.1 to Pic.3.5 are some pictures that depict the actual set up and apparatus for fabricating FBG.

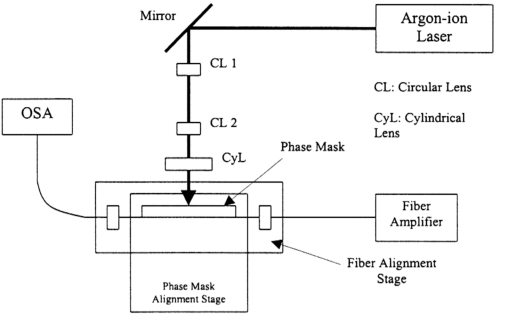

Figure 3.1: FBG fabrication system set up

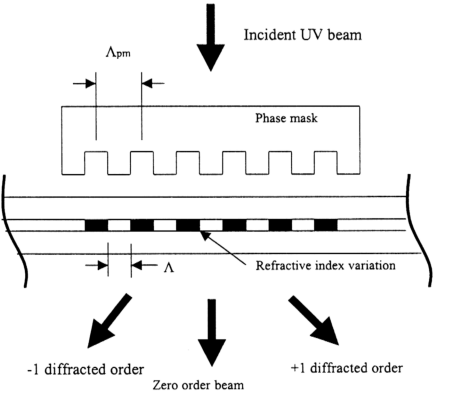

Figure 3.2: Grating formation using phase mask

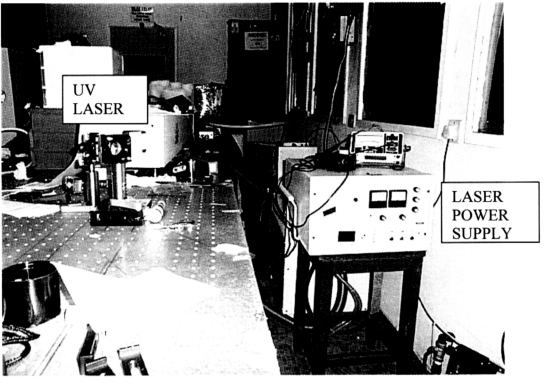

Pic.3.1 : UV laser placement in the set-up. The UV output is blocked from view by a mirror and a lens. On the right is the laser power supply.

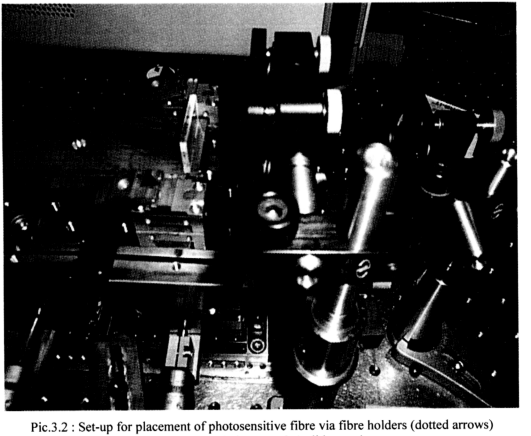

Pic.3.2 : Set-up for placement of photosensitive fibre via fibre holders (dotted arrows) and phase mask (solid arrow)

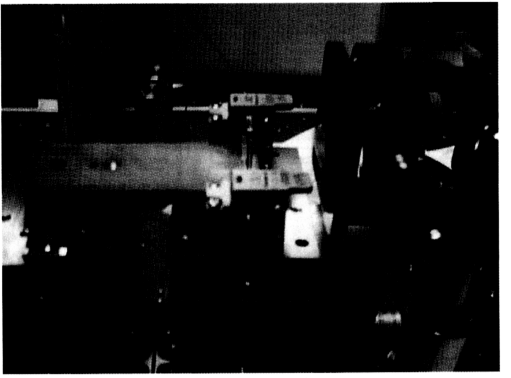

Pic.3.3: A view of phase mask, fiber and cylindrical lens during fabrication process

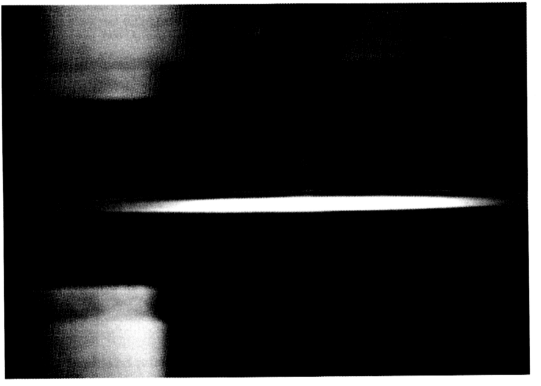

Pic.3.4: A photosensitive fibre at the focus of UV radiation of wavelength 244nm. The glowing streak is due to too high intensity of UV causing the CCD camera to saturate.

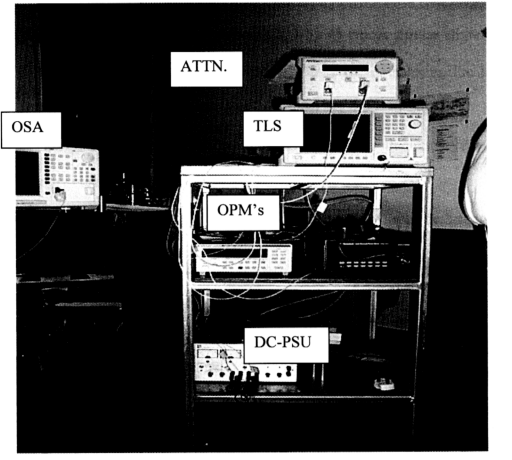

Pic.3.5 : Fabrication measurement set-up. To the extreme left is an Optical Spectrum Analyser (OSA) and on the rack is the DC supply for an Optical Amplifier (OA), two Optical Power Meters (OPM), a Tunable Laser Source (TLS) and an Attenuator.

3.3 Alignment method

The Argon ion laser is turned on after its cooling water system has been running for 30 minutes and nitrogen gas has been flowing into the laser cavity for at least 5 minutes. Then it is aligned to get a maximum power between 80 to 100 mW at a tube current of 20A. A mirror placed in the light path reflects the light and its height is aligned by adjusting this mirror. A circular lens CL 1 is set perpendicular to the laser beam; its perpendicularity confirmed by observing reflected light from the lens at the laser head. The reflected laser beam must be on the same place from where it was launched as shown on Pic.3.6. Pic.3.7 shows that the lens is not aligned properly since the spot of the reflected beam is not at its proper place. A second circular lens,

CL 2 is placed on the set up, separated from CL 1 by 45 cm. A similar alignment as for CL 1 is done to ensure the lens is perpendicular to the laser beam. Pic.3.8 and Pic.3.9 show the position of aligned and unaligned CL 2, respectively. It is also extremely important to ensure that the beam hits the center of both circular lenses; this is confirmed by observing the Boys image.

Once the beam has been expanded and collimated by telescopic arrangement of CL 1 and CL 2, a cylindrical lens is placed to focus the laser beam horizontally. A line of reflected light can be observed on the laser exit and it must be adjusted to be reflected onto the laser exit hole as shown in Pic.3.10. Then the phase mask is put in. Its position is aligned to be perpendicular to the laser beam by observing the reflected light. The light must be placed on the laser exit hole as shown in Pic.3.11. The phase mask corrugations must be put horizontally against the cylindrical lens, which can be adjusted by observing the transmitted light from the phase mask. Pic.3.12 and pic.3.13 show a view of the phase mask aligned and unaligned, respectively, when the light irradiates the upper boundary of the corrugations. The bare fiber is settled parallel to the phase mask edge far from contact with the fine corrugations. The shadow of the fiber is observed to fine tune the alignment of its position. Pic.3.14 and Pic.3.15 show both first orders of diffracted light when the fiber is aligned and unaligned, respectively.

Once the fiber position is aligned properly, the laser power is reduced to very low level and the fiber is brought to near contact with the fine corrugations of the phase mask. Its separation is adjusted to be almost in contact with phase mask. The fiber position is reconfirmed again. If the alignment is perfect, the fabrication can be initiated. The shadow of light during fabrication process for perfect alignment is shown in Pic.3.16.

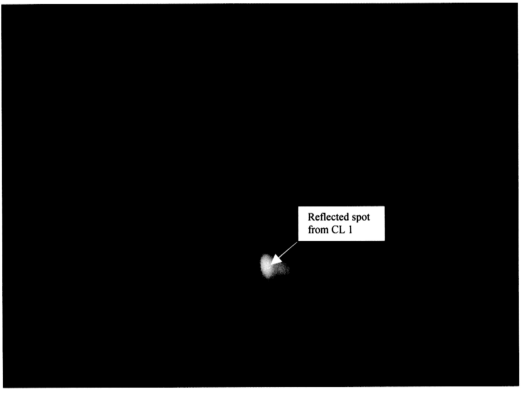

Pic.3.6: The spot of reflected light for aligned CL 1 lens.

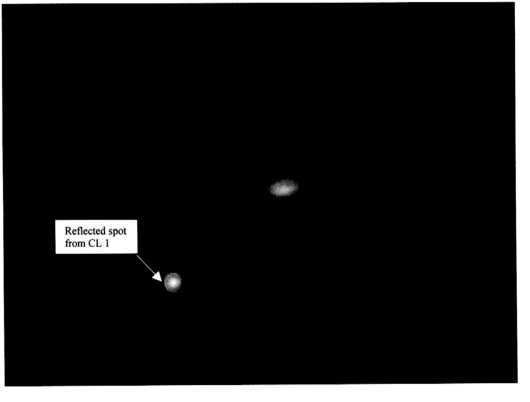

Pic.3.7: The spot of reflected light for unaligned CL 1 lens.

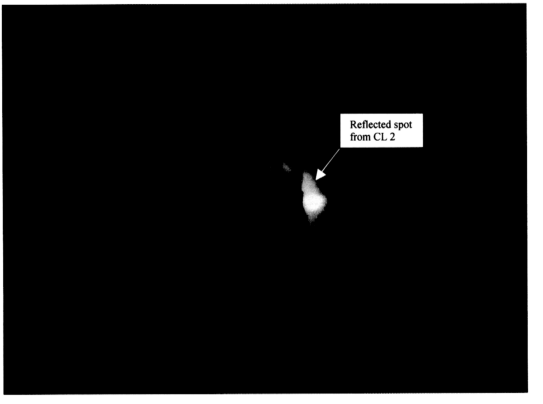

Pic.3.8: The spot of reflected light for aligned CL 2 lens.

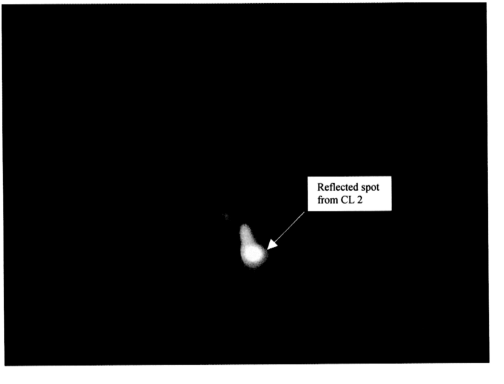

Pic.3.9: The spot of reflected light for unaligned CL 2 lens.

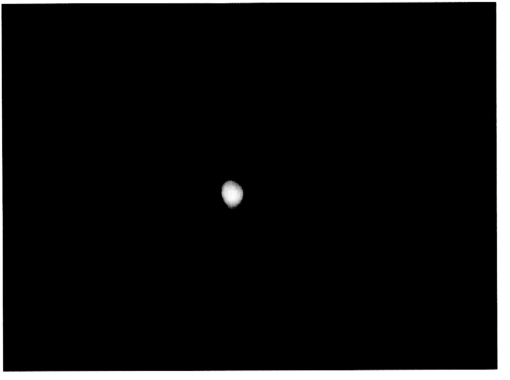

Pic.3.10: The line of reflected light for aligned Cy lens.

Pic.3.11: The line of reflected light for aligned phase mask.

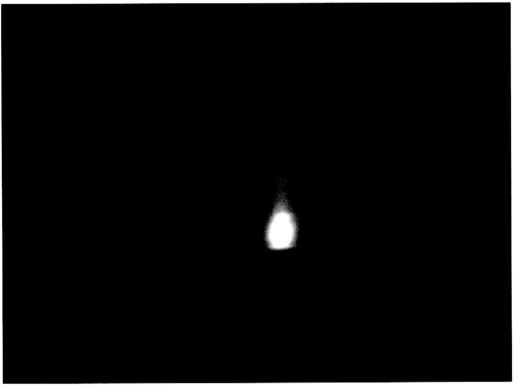

Pic.3.12: The diffracted light from the aligned phase mask.

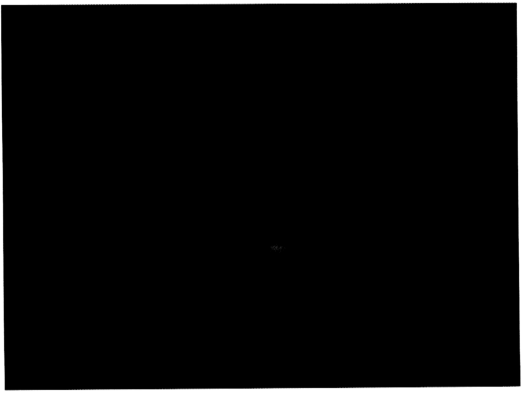

Pic.3.13: The diffracted light from the unaligned phase mask.

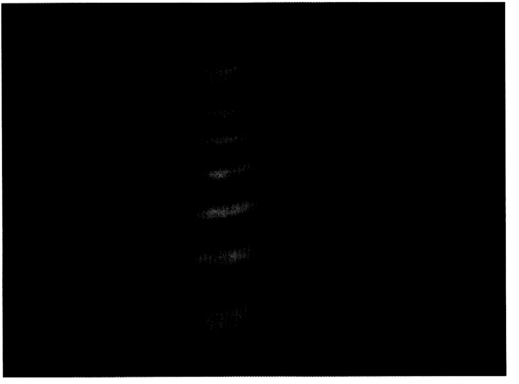

Pic.3.14: The first order diffracted light when the fiber aligned.

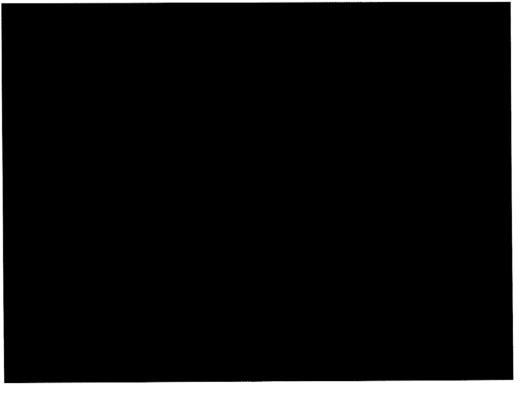

Pic.3.15: The first order diffracted light when the fiber unaligned.

Pic.3.16: The diffracted light during fabrication.

3.4 Advantages of high-germania boron-codoped fiber

The sensitization of UV-induced refractive index changes is of importance in the production of fiber Bragg grating. The use of boron as codopant in germanosilicate fibers and hydrogenation are well-established photosensitization methods. A high-germania boron-codoped fiber is used to inscribe FBG in our experiment. The parameters of the fiber are summarized in Table 3.1. In the past, fibers have been photosensitized either by increasing their germania content or by hydrogenation. The addition of GeO_2 into the fiber core tends to increase the index and compensation is via core size reduction in order to preserve the fiber NA. However small core of high germania fiber makes them incompatible with standard communication fibers. On the other hand, hydrogenation not only adds complexity and cost but also tends to produce high loss gratings after UV irradiation. The high-

germania boron co-doped fiber has been designed to be both intrinsically photosensitive and compatible (in terms of mode-field diameter) with conventional telecommunications fibers. In this way, not only high-performance gratings can be written without hydrogenation, but also splice it to standard fibers easily and with low loss.

Table 3.1: High germania boron co-doped fiber parameters

Design Wavelength	1550nm
Cut-off Wavelength	1250nm ~ 1500nm
Numerical Aperture	0.11 ~ 0.13
Outside Diameter (Fiber)	125μm ± 1%RMS (<3% peak)
Outside Diameter (Coating)	245μm ± 5%
Proof Test	0.5% strain (50 kpsi)

The fiber uses a combination of boron and germania within the fiber core in order to achieve this performance. In essence, the germania provides the photosensitivity but raises the index and addition of boron acts to depress the index down to 'telecoms' levels and reduces the time taken for the grating to be written.

3.5 The phase mask

A major step toward easier inscription of FBGs is made possible by the application of the phase mask as a component of the interferometer. The phase mask is a one-dimensional periodic surface relief grating. Most phase masks are fabricated by e-beam lithography on a fused silica plate. But the phase mask used in the experiments herein is fabricated by UV-laser interferometer and is optimised for

244nm. Its other parameters are summarized in Table 3.2. It is a square shaped binary phase grating.

Table 3.2: Parameters of the phase mask

Material		SiO2
Grating Period		1.0726μm
Clear aperture		30mm
Diameter		38.1mm
Diffraction Efficiencies	+1 order	36.4%
	0 order	1.2%
	-1 order	36.5%

The UV laser beam passing through the phase mask is diffracted to form a three-dimensional interference pattern, which is useful for photo-imprinting the FBG. With the UV radiation at normal incidence, the diffracted radiation is split into m = 0 and ±1 orders, as shown in Figure 3.2. The interference pattern induces a refractive index modulation in the core of the photosensitive fiber. The phase mask technique is superior to the interferometer [3] and point-by-point methods of writing FBGs due to its simplicity and reduced mechanical sensitivity.

3.6 Laser source

There are several laser sources that may be used for inducing refractive index change and for fabricating FBGs in optical fibers which can be classed as pulse laser and CW laser. The most common UV pulse sources used to fabricate FBGs with a phase mask are 248nm KrF and 193nm ArF excimer laser. They have high UV power

and a beam diameter of a few centimeters, but low spatial and temporal coherence. Fabrication becomes easy with these lasers due to its high power and large beam size. Meanwhile a 244nm frequency doubled Argon ion CW laser has a high spatial and temporal coherence, but with smaller power and beam diameter. The inscription is harder with this laser due to alignment problems caused by the smaller beam and laser power.

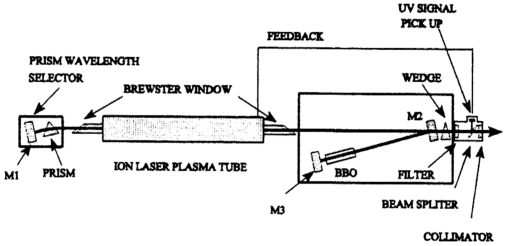

Figure 3.3: Configuration of Argon ion laser system cavity with internal harmonic generator (BBO)

In the experiments described herein, a continuous wave (CW) ultraviolet laser is used to inscribe FBGs. The laser is an intracavity frequency doubled Argon ion laser. The system produces deep UV CW output, at a wavelength of 244nm with high conversion efficiency, long lifetime and good beam quality. Its excellent performance has been proven in both basic research and industrial applications. Figure 3.3 shows the laser system cavity configuration. It is a three mirror folded cavity. M1 is a high reflector for visible wavelengths between 450~550nm. A prism wavelength selector is used to select the single line fundamental wavelength. The folding mirror, M2, is a curved dichroic mirror. It reflects the fundamental completely and focuses the

intracavity fundamental beam on the BBO crystal. M2 also acts as an output coupler for the transmitted UV output. The end mirror, M3, reflects the fundamental back to the plasma tube. This cavity allows for a large TEM_{00} mode volume in the ion laser plasma tube and provides a high power density in the nonlinear crystal.

The maximum output power of the laser is 100mW at 20A. The beam diameter of the laser is 1.191 mm with divergence of 0.56 mrad. The beam profile of the laser is measured as follows. The pinhole is placed in position with a photodiode behind it. The amount of light was measured with a precision multi-meter connected to the photodiode. The measured vertical and horizontal distribution of beam profiles are shown in Figure 3.4 and 3.5, respectively. Figure 3.4 shows that there are two peaks in the vertical profile which are separated by 0.8 mm after focusing. The beam profile is fitted and verified that it has a Gaussian distribution profile. The solid curves in Figure 3.5 are obtained by fitting the UV intensity with a Gaussian form.

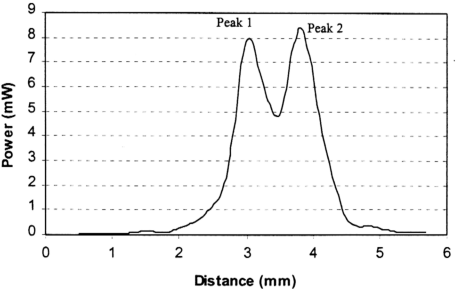

Figure 3.4: The vertical distribution of laser beam profile

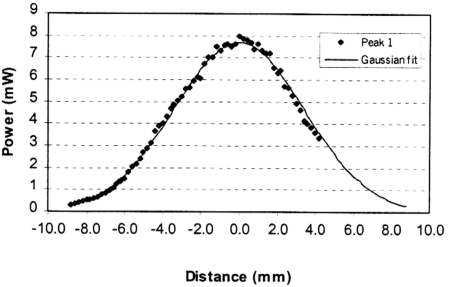

(a) Peak 1

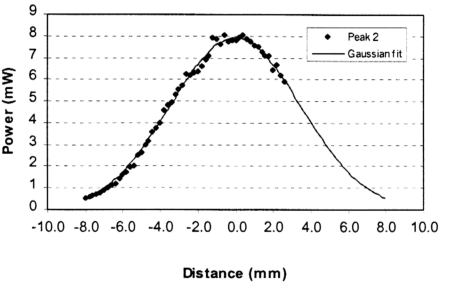

(b) Peak 2

Figure 3.5: The horizontal distribution of laser beam profile (a) peak 1 (b) peak 2

The Gaussian beam is expected to contribute to side-lobes in the fabricated gratings. It is understood from the vertical beam profile that the peak 2 is higher than peak 1. So, the fiber should be brought to peak 2 during fabrication process.

3.7 Growth characteristics of FBG

The FBG growth in high germania boron co-doped single mode fiber have been monitored during exposure time. For the fabrication set up used, the growth rates of the fabricated FBGs measured by an OSA are shown in Figure 3.6. The laser power at the laser exit was about 80 mW. The fastest growth rate is shown by FBG 1. Its measured transmission loss reached 30.3 dB which translates to reflectivity of 99.9% in an exposure time for 524 sec. The difference in the growths is attributed to slight differences in alignment for the FBGs.

The growth in back reflected light is explained in terms of a new nonlinear effect called "photosensitivity" which enables an index grating to be written. The photosensitivity of optical fiber is due to defect formation inside the Ge-doped core of

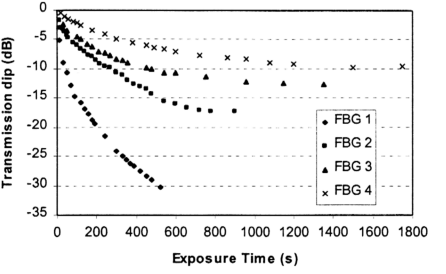

Figure 3.6: The growth rates of the FBGs

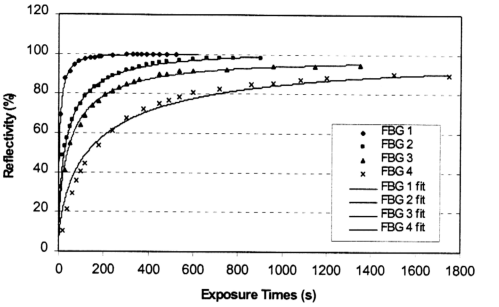

Figure 3.7: The FBGs reflectivity as a function of exposure time

silica fiber [6]. The presence of Ge atoms leads to formation of oxygen-deficient bonds (such as Si-Ge, Si-Si, and Ge-Ge) which act as defects in the silica matrix. The most common defect is the so-called GeE' defect. The GeE' is a hole trapped next to a germanium at an oxygen atom [7]. It forms a defect band with an energy gap of about 5 eV (energy required to break the bond). Single absorption of 244 nm radiation from a frequency doubled Argon ion laser breaks this defect bond, and the released electrons are trapped at hole-defect sites to form color centers such as Ge(1) and Ge(2). Resulting changes in the absorption spectrum are accompanied by a corresponding index change through the Kramers-Kronig relation [8]. Since index changes occur only in the regions of fiber core where the UV light is absorbed, a periodic intensity pattern is transformed into an index grating. The coherent light propagating in the fiber interferes with a small amount of light reflected back from the end of the fiber to set up a standing wave pattern, which through photosensitivity writes an index grating in the core. As the strength of FBG increases, the intensity of

back-reflected light increases until it saturates near 100%. The growth rate is considered to be proportional to the relative difference Δn related with germanium concentration.

Gilbert S. L *et al.* [2] explained a simple model of grating growth arising from the depletion of a homogeneously broadened defect population by one-photon absorption. That model predicts an exponential growth of the index to a maximum value corresponding to the complete depletion of the defects. The dependence of Δn on the time and intensity is given by

$$\Delta n = \Delta n_{max}[1 - \exp(-AIt)] \tag{3.1}$$

where Δn_{max} is the index change that would be produced if the defect population were fully depleted, t is the UV exposure time, I is the intensity of the UV light, $A = \sigma / h\upsilon$, and σ is absorption cross section and $h\upsilon$ is the energy of a 244nm photon. This equation assumes that the grating is in early stages of growth. For exposure times long enough to saturate the index change, however, the reflectance is expected to reach a maximum and then decrease to zero as the defects in the low intensity regions are depleted. However, they observed that the dependence of index modulation on time and intensity does not agree with the predictions of the model.

The reflectivity R of the fabricated FBG is given by

$$R = \tanh^2 [(\eta\pi L\Delta n)/\lambda], \tag{3.2}$$

where η is the fraction of the single mode intensity contained in the core and L is the grating length. Figure 3.7 shows the FBGs reflectivity as a function of fabrication time calculated from Figure 3.6. The solid curves are obtained by fitting Δn to a power law of the form $\Delta n = Ct^b$, and inserting this dependence into equation (3.2). The fit given by the power law is very good, whereas an exponent b of 0.3 is obtained for the FBGs. The power law dependence of Δn is produced by an inhomogeneous

broadening of the defect population. The CW light is found to produce a smaller index change than pulsed light for the same type of fiber and comparable UV fluence [2]. This difference in writing efficiency is related to transient heating or compaction of the glass matrix as a result of the high peak intensity of the pulsed light.

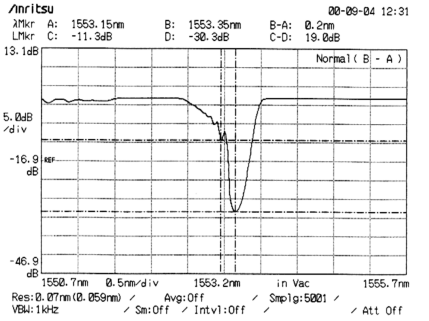

Figure 3.8: Transmission spectrum of the FBG 1

The measured transmission spectrum of the FBG 1 after 524 s exposure by our fabrication method is shown in Figure 3.8. It has a dip of –30.3 dB, which translates to 0.1% of the incoming signal at this particular wavelength will go through, and a bandwidth of 0.16nm centered at 1553.3 nm. The well known condition for the Bragg reflection wavelength λ_B is given by the expression

$$m \lambda_B = 2 n_{eff} \Lambda \tag{3.3}$$

where m is the reflection order number, n_{eff} is the effective refractive index of the fiber core and Λ is the period of the grating. Using the known Sellmeier coefficients, n_{eff} at 1553.3 nm is calculated to be 1.444. This then predicts that a first-order reflection at

1553.3 nm should be given by a 538 nm period grating, which is within 1% of the period predicted to be produced by the phase mask period. The grating period is predicted to be half of the phase mask period. This discrepancy is thought to arise from variations in the depth and uniformity of the etched lines on the phase mask.

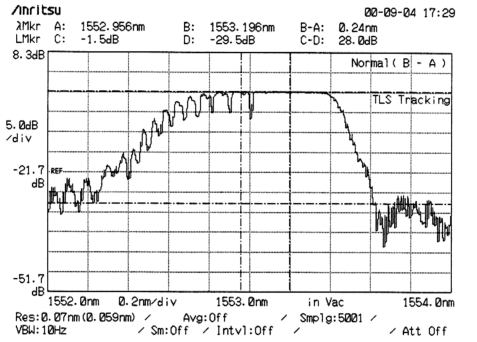

Figure 3.9: Reflection spectrum of the FBG 1

The measured reflection spectrum of the FBG 1 after 524s exposure is shown in Figure 3.9. It has a full bandwidth to the first zeroes of 1.4nm. The bandwidth and strength of the reflection depend on the index change per period and the overall length of the grating. The maximum reflection strength is given by

$$R_{max} = \tanh^2(\kappa L) \tag{3.4}$$

where κ is coupling coefficient and L is grating length. Assuming that all of incoming lights which do not transmitted were reflected back, so the maximum reflectivity is

calculated to be 99.9% from the transmission spectrum. Then, the κL is calculated to be 4.1468 from equation (3.4). The full bandwidth to the first zeroes is given by

$$\Delta\lambda = \lambda_B^2[(\kappa L)^2+\pi^2]^{1/2} / \pi n_{eff} L \qquad (3.5)$$

From this equation, the grating length is calculated to be 1.976 mm by substituting κL = 4.1468, λ_B=1553.3, Δλ=1.4nm and n_{eff} = 1.444. Then, the coupling coefficient κ is calculated to be 2098.2 from equation (3.4). Based on measurements, however, the grating length should be more than 1cm, a fact attributed to the grating strength. The above formulae are not accurate for strong gratings but are used as a guide for analysis.

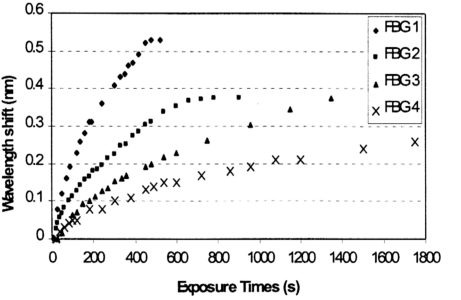

Figure 3.10: Transmission wavelength drift with fabrication time

Although the phase mask limits the wavelength that can be reflected in the fiber, however, there are effects of the UV laser light that cause a drift of the resonance wavelength with fabrication time. Figure 3.10 shows the change of Bragg reflection wavelength with fabrication time, which increases in tandem with Bragg

reflection strength for the fabricated FBGs. The fastest wavelength shift is shown by FBG 1. Its wavelength is shifted roughly by 0.53 nm after 524 seconds exposure. We assume that the shift is mainly due to a variation of the core index of the optical fiber averaged over the irradiated region that arises from the unmodulated component of the UV induced index change. Other mechanisms could explain a grating wavelength shift. For instance, it can be assumed that, owing to residual curvature of the wave front impinging on the phase mask, there is a slight increase of the grating period from the edge of the grating where the interference order is minimum to the other edge where the interference order is maximum. Because the intensity and the visibility of the interference pattern decrease when the interference order increases [9], a possible saturation and/or threshold of the writing may lead not only to an asymmetry and to a broadening of the spectral shape but also to a positive shift in the resonance wavelength of the grating as the fabrication time is increased.

In case of misalignment such that the fiber is not set perpendicular to the phase mask, a high reflectivity FBG will not be obtained. One of these FBG growths is shown in Figure 3.11. The reflectivity increases with fabrication time until it reaches 83% and then starts to reduce. The grating fringes in the core could be tilted by this misalignment. Grating tilt affects the coupling to radiation modes, which reduces the maximum reflectivity of the grating. The tilted grating also affects Bragg reflection by effectively reducing the fringe visibility. The maximum reflectivity becomes lower as the visibility is reduced. However, this effect is considered very small, since the CW argon ion laser has an intrinsically high spatial and temporal coherence. Proper use of tilt for reducing the effective visibility and hence, Bragg reflection can be practically useful in cases where large radiation or other bound mode coupling is desired but Bragg reflection is undesirable [10].

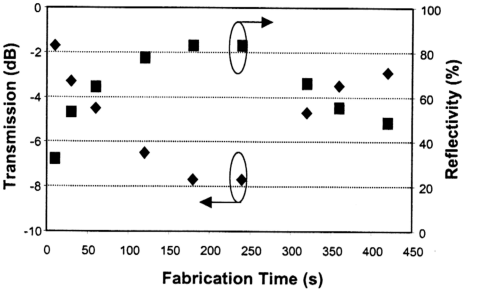

3.11: FBG growth as a function of fabricating time for bad alignment

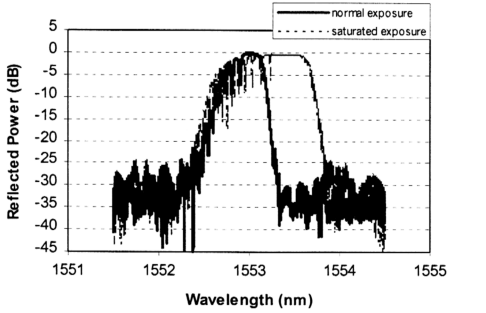

Figure 3.12: FBG spectrum bandwidth for different exposure

In FBG fabrication, the growth of transmission or reflection spectra should be monitored during UV exposure. The exposure should be stopped the moment it reaches saturation. When a grating is formed with a saturated exposure, then the effective length will be reduced as the transmitted signal is depleted by reflection. As a result, the spectrum will broaden appreciably and depart from a symmetric shaped spectrum whose width is inversely proportional to the grating length. The spectrum broadens because the incident wave is completely reflected before reaching the end of the grating. A strongly saturated grating is no longer sinusoidal, the peak index regions are flattened and the valleys in the perturbation index distribution are sharpened. As a result, second order Bragg reflection line can be observed at about one-half the fundamental Bragg wavelength and at other shorter wavelength for higher order modes, however these are not of interest in the current work. Figure 3.12 shows the FBG spectrum bandwidth for different exposures. The bandwidth of the fabricated FBG with saturated exposure is broader than the unsaturated FBG.

3.8 Cladding modes

Improvements in grating fabrication methods and enhancements in fiber photosensitivity have led to significantly stronger refractive-index modulation. As a result, a series of cladding mode coupling resonance appears in the FBG transmission spectrum at wavelengths below the Bragg peak [11]. Figure 3.13 and 3.14 show a transmission and reflection spectrum at short wavelength side of one of our FBG, respectively. A series of transmission dip appears in the transmission spectrum, but nothing is seen in the reflection spectrum. The reflection spectrum cannot detect the cladding mode due to background noise levels being higher than loss caused by the

cladding modes. This transmission dip also is called a ghost grating because it is comparable in size to the Bragg reflection dip.

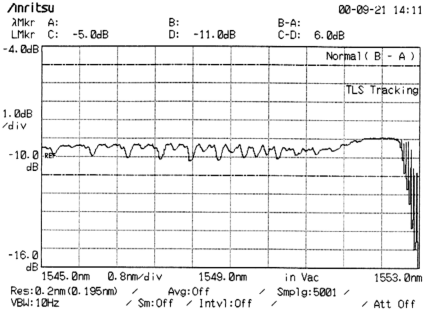

Figure 3.13: Transmission spectrum on short wavelength side

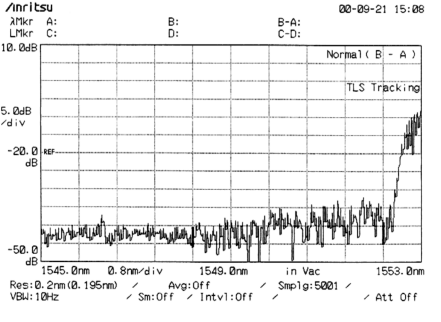

Figure 3.14: Reflection spectrum on short wavelength side

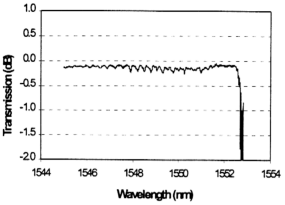

(a) Reflectivity of 87.7%

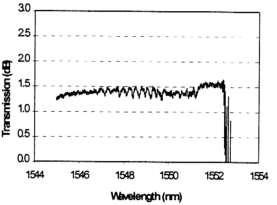

(b) Reflectivity of 97.5%

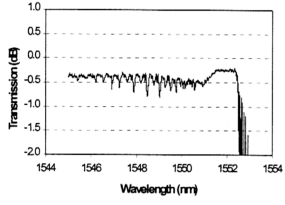

(c) Reflectivity of 98.9%

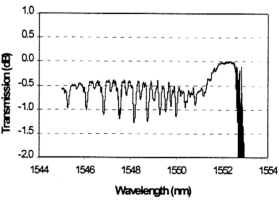

(d) Reflectivity of 99.9%

Figure 3.15: The cladding modes on transmission spectrum of the fabricated FBGs

Figures 3.15(a) ~ (d) are transmission spectra for discrete reflectivities of various fabricated FBG's. All gratings show a series of fine structure features on the short-wavelength side of the fundamental Bragg line. The cladding mode spacing from main mode for these spectra is within 1.9 ~ 2.4nm. The ghost grating transmission dip as a function of FBG reflectivity is shown in Figure 3.16. A higher reflectivity causes a more severe cladding mode in the FBG. The fine structure features are caused by wave coupling between the guided fundamental mode LP_{01} and

modes within the cladding in a FBG. UV absorption effects will cause an asymmetry in the UV-induced index, which in turn will cause a ghost grating dip to appear. This can arise from an asymmetry of transverse absorption of UV light during writing.

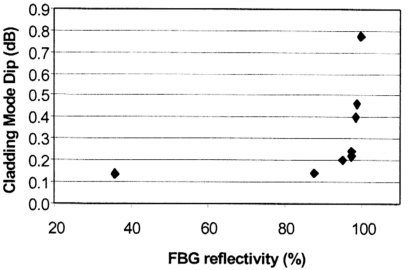

Figure 3.16: cladding mode transmission dip as a function of FBG reflectivity

The cladding mode renders these gratings unusable in wavelength-division multiplexed systems or where the short wavelength side of gratings is used such as pumping fiber lasers. Several methods have been proposed to suppress coupling to cladding mode. The cladding mode loss problem can be reduced by having a photosensitive cladding [12]. The principle is that the orthogonality of the modes will eliminate the intermodal coupling if a uniform refractive index change over the wave front of the guided mode is produced in a grating. The cladding mode loss can also be reduced by using special fibers. One special fiber uses a depressed cladding around the core region [13]. This depressed cladding very effectively reduces the field strength of cladding modes over the core region and therefore reduces the coupling from the guided fundamental mode to leaky cladding modes. Another design has a

small core and high NA that moves the cladding modes to shorter wavelengths by over 10 nm from the central peak of the grating [14].

3.9 Side lobes

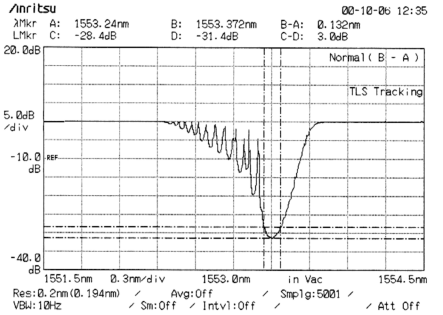

Figure 3.17: The side lobes on the short wavelength side

One of the transmission spectra of FBG fabricated in these experiment is presented in Figure 3.17. The FBG presents an undesirable fine structure on the short wavelength side. These structures are called sidelobes and it happens due to a non-uniform average index change [11]. The non-uniform average index is caused by a Gaussian profile of UV beam distribution along the fiber axis and it leads to self-induced chirp in the grating period. This chirp causes the resonant wavelength on either end of the grating to be smaller than the resonant wavelength of the central portion of the grating, setting up Fabry-Perot resonance, which manifest as sidelobes

on the lower wavelength side. These side lobes do not occur if the average index change is held constant or adjusted to be constant.

This FBG is not desirable for use in WDM systems applications because the presence of the sidelobes increases the frequency separation (guard-space) needed between optical carriers to reduce interchannel interference to acceptable levels. To suppress the sidelobes caused by self-induced chirp, it is necessary to keep the average refractive index constant along the grating while a smoothly changing amplitude profile is placed on the grating exposure. Various efforts have been reported in the literature to get rid of this short wavelength resonance, some with very promising results, but most of them are besieged by issues like high cost, difficulty in implementation or inherently slow grating fabrication times. As an example, Malo *et al* [15] demonstrated a double exposure method by using shadow masks to control the index variation along the grating, Cole et al [16] used a 'moving fiber / phase mask-scanning beam' technique for enhanced flexibility in producing fiber gratings, while Yang and Lai [17] used an apodized phase mask with a Gaussian UV beams to fabricate a steep skirt fiber Bragg grating.

3.10 Apodization

Apodization refers to a reduction of the secondary maxima in the FBG reflection response. It is achieved by photoinducing a refractive index grating with a modulation amplitude that has a bell-like functional shape along the grating length. Typical apodization functions are Gaussian, super gaussian, cosine squared, sinc, Hamming, etc. A simple Gaussian apodization can eliminate side-lobes, but does not create steep skirts desired for WDM applications and requires a longer length grating to cover the long taper. Cosine apodization improves the skirt steepness and length

problem, but increases the side-lobe level somewhat. For low reflectivities (<50%) the grating spectral response is approximately the Fourier transform of the exposure profile. Thus, a sinc function apodization will produce a grating with a rectangular spectral response. This apodization requires π phase change at the nulls of the function to produce an effective negative response. An exact rectangle response cannot be achieved since the sinc series must be terminated at some point. Unfortunately, this apodization does not work well at higher reflectivities. Development work is underway to solve this problem.

Our experimental configuration in Figure 3.1 is extended to fabricate an apodised FBG using apodised phase mask. Pic.3.17 to Pic.3.19 are some pictures that depict a view of the diffraction pattern of 244nm UV light due to an apodised phase mask. The apodised phase mask has a period of 1.0726 for 244nm wavelength. The reflection spectrum of the fabricated apodised FBG is shown in Figure 3.18. It has a center wavelength of 1552.6nm, a 3dB bandwidth of 0.11nm and a peak reflectivity of 27%. The side lobe only appears at wavelengths –0.2nm from the center wavelength with the reflection is 24dB lower than the peak reflectivity. In this apodised FBG, the average local refractive index has been corrected so that the local Bragg resonance is constant along the whole length of the grating. The reflection spectrum of this apodised FBG has shown a smaller bandwidth and a nicer shape compared to the spectrum of the unapodised FBG fabricated in the previous configuration.

The issues related to the apodised phase mask, although desirable, is limited in flexibility by allowing only the replication of the type of apodization programmed in the phase mask. There is a restriction on the maximum size of the phase mask as well as the reproducibility of the apodised phase mask. Other well-known techniques to produce apodization are a multiple printing in-fiber (MPF) method [18] and a moving

fiber/phase mask (MPM) method [19], [20]. In the MPF method, a series of overlapped gratings are written. This method relies on the fiber being translated across an interference fringe pattern in synchronism with the arrival of UV writing pulse. It is possible with a pulsed UV laser system and requires extreme precision in positioning the fiber. For MPM writing method, the fiber is moved along with the phase mask in front of a stationary UV beam, or with the UV beam scanned across a fixed phase mask, with the fiber moving slowly relative to phase mask. Both the MPF and MPM methods are flexible and capable of apodizing gratings with arbitrary refractive index modulation profiles and are capable of the production of identical grating characteristics.

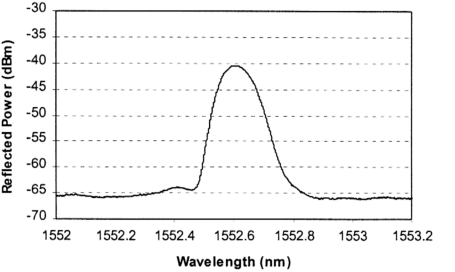

Figure 3.18: The reflection spectrum of the fabricated apodised FBG. It has a reflectivity of 27% with center wavelength at 1552.6 and FWHM of 0.11nm.

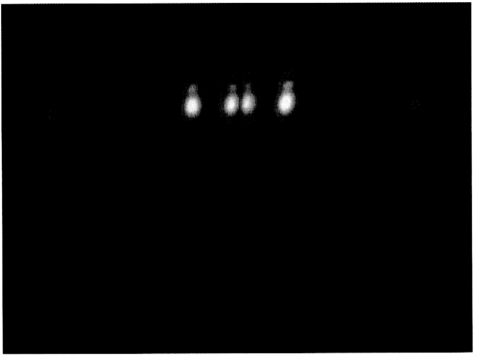

Pic.3.17: Diffraction pattern of 244nm UV light due to an apodised phase mask.

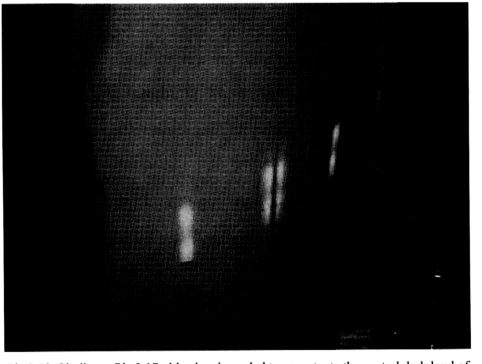

Pic.3.18: Similar to Pic.3.17, this view is angled to accentuate the central dark loud of the 0th order diffraction pattern from the apodised phase mask.

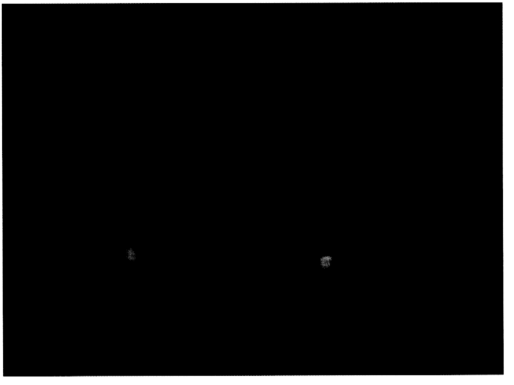

Pic.3.19: A view of the diffracted light from the unaligned fiber during fabrication of apodised FBG.

References

1. C. Askin, M. A. Putnam, G. M. Williams and E. J. Friebele, "Fibre optic reflectors prepared by single excimer pulse," Opt. Lett., Vol. 17, pp. 833-835, 1992.
2. H. Patrick and S. L. Gilbert, "Growth of Bragg gratings produced by continuous-wave ultraviolet light in optical fiber," Opt. Lett., Vol. 18, No.18, pp.1484, 1993.
3. G. Meltz, W. W. Morey and W. H. Glen, "Formation of Bragg gratings in optical fibres by a transverse holographic method," Opt. Lett., Vol. 14, pp. 823-825, 1989.
4. B. Malo, K.O. Hill, F. Bilodeau, D. C. Johnson and J. Albert, "Point-by-point fabrication of micro Bragg gratings in photosensitive fiber using single

excimer pulse refractive index modification technique," Electron. Lett., Vol. 29, No. 18, pp. 1668-1669, 1993.

5. K. O. Hill, B. Malo, F. Bilodeau, D. C. Johnson and J. Albert, "Bragg gratings fabricated in monomode photosensitive optical fibre by UV exposure through a phase mask," Appl. Phys. Lett., Vol. 62, pp. 1035-1037, 1993.

6. G. Meltz and W. W. Morey, " Bragg grating formation and germanosilicate fiber photosensitivity," SPIE Proc. 1516, 185-199, 1991.

7. T. E. Tsai, D. L. Griscom, E. J. Fribele and J. W. Fleming, "Radiation induced defect centers in high purity GeO_2 glass," J. Appl. Phys., 62, pp. 2262-2268, 1987.

8. P. N. Butcher and D. Cotter, "Elements of Nonlinear Optics," Cambridge University Press, Cambridge UK, 1990.

9. M. Douay, S. Canon, S. Legoubin, E. Fertein, P. Bernage, P. Niay and J. F. Bayon, "Formation of Bragg gratings in germanium doped optical fibers using a prism interferometer," 2nd Int. Conf. Grenoble, 1991.

10. T. A. Strasser, J. R. Pedrazzani and M. J. Andrejco, "Reflective mode conversion with UV-induced phase gratings in two-mode fiber," in Optic. Fiber Commun. Conf., Dallas, TX, paper FB3, 1997.

11. V. Mizrahi and J.E. Sipe, "Optical properties of photosensitive fiber phase gratings," J. Lightwave. Tech., Vol. 11, pp 1513, 1993.

12. E. Delevaque, S. Boj, J.F. Bayon, H. Poignant, J. Le Mellot, and M. Monerie, "Optical fibre design for strong gratings photoimprinting with radiation mode suppression," OFC, paper PD5, 1995.

13. L. Dong, L. Reekie, J.L. Cruz, J.E. Caplen and D.N. Payne, "Cladding mode coupling suppression in fibre Bragg grating using fibres with a depressed cladding," ECOC, Oslo, paper MoB.3.3, 1, pp. 53-56, 1996.

14. T. Komukai and M. Nakazawa, "Efficient fibre gratings formed on high NA dispersion-shifted fibres," ECOC, paper MoA3.3, 1, pp.31-34, 1995.

15. B. Malo, S. Theriault, D. C. Johnson, F. Bilodeau, J. Albert and K. O. Hill, "Apodised in-fibre Bragg grating reflectors photoimprinted using a phase mask," Elec. Lett., Vol.31, No.3, pp.223-225, 1995.

16. M. J. Cole, W. H. Loh, R. I. Laming, M. N. Zervas and S. Barcelos, "Moving fibre / phase mask-scanning technique for enhanced flexibility in producing fibre gratings with uniform phase mask," Elec. Lett., Vol 31, No. 3, pp.1488-1490, 1995.

17. C. Yang and Y. Lai, "Improving the spectral sharpness of an apodized fibre grating," J. Opt. A : Pure Appli. Opt., 2, pp.422-425, 2000.

18. R. Stubbe, B. Sahlgren, S. Sandgren and A. Asseh, "Novel technique for writing long superstructured fiber Bragg gratings," in *Photosensitivity and Quadratic Nonlinearity in Glass Waveguides: Fundamentals and applications*, Vol. 22, 1995 OSA Technical Series (Optical Society of America, Washington DC), PD1-(1-3), 1995.

19. M. J. Cole, W. H. Loh, R. I. Laming, M. N. Zervas and S. Barcelos, "Moving fiber/phase mask-scanning beam technique for enhanced flexibility in production fiber gratings with a uniform phase mask," Electron. Lett., 31(17), pp. 92-94, 1995.

20. M. J. Cole, W. H. Loh, R. I. Laming, M. N. Zervas and S. Barcelos, "Moving fiber/phase mask-scanning beam technique for writing arbitrary profile fiber

gratings with a uniform phase mask," in *Photosensitivity and Quadratic Nonlinearity in Glass Waveguides: Fundamentals and applications*, Vol. 22, 1995 OSA Technical Series (Optical Society of America, Washington DC), PD1-(1-3), 1995.